Advances in Water Resources 143 (2020) 103658

Contents lists available at ScienceDirect

Advances in Water Resources

journal homepage: www.elsevier.com/locate/advwatres

Flow of shear-thinning fluids through porous media

Christophe Airiau[a], Alessandro Bottaro[b,*]

[a] Institut de Mécanique des Fluides de Toulouse (IMFT), Université de Toulouse, CNRS, INPT, UPS, Toulouse, France
[b] DICCA, Scuola Politecnica, Università di Genova, via Montallegro 1, 16145 Genova, Italy

ARTICLE INFO

2019 MSC:
76A05
76S05
78M40

Keywords:
Porous media
Homogenization
Adjoint theory
Carreau fluids

ABSTRACT

Pseudo-plastic fluids exhibit a non-linear stress-strain relationship which can provoke large, localized viscosity gradients. For the flow of such fluids in porous media the consequence is a strong variability of the effective permeability with porosity, angle of the macroscopic pressure gradient, and rheological parameters of the fluid. Such a variability is investigated on the basis of adjoint homogenization theory for a Carreau fluid in an idealized porous medium geometry, highlighting differences with respect to the Newtonian case. It is shown in particular that the more we depart from Newtonian conditions, the more the (often used) hypothesis of an effective viscosity in Darcy's law is a poor approximation, for the effective permeability tensor becomes strongly anisotropic.

1. Introduction

Fluids whose apparent viscosity decreases under shear strain are very common, and are often found in polymer and foam solutions; also complex fluids and suspensions like ketchup, paints and blood exhibit such a property which goes by the name of shear-thinning or pseudo-plasticity. The oldest model used to describe the rheological properties of pseudo-plastic fluids is the empirical power-law equation (Ostwald, W. (1925, 1929)) which relates the shear stress to the shear rate elevated to a certain power, say n, with $n < 1$, via a coefficient called the flow consistency index. For $n = 1$ the Newtonian behavior is recovered. The simple power-law behavior yields infinite effective viscosity as the applied stress vanishes, and this can cause numerical difficulties in applications, which is why more elaborate models have later been proposed, such as the Carreau, Carreau-Yasuda, Cross or Powell-Eyring models (Bird, R.B., Armstrong, R.C., Hassager, O. (1987); Tanner, R.I. (2000)). All of these models are reasonably simple to implement (for example in a numerical code), requiring no more than three empirical constants; they all yield rather good results, provided the fitting parameters are well chosen, as shown in Fig. 1 for a representative engine oil in solution with viscosity-index-improver polymers (Marx, N., Fernández, L., Barceló, F., Spikes, H. (2018).

Several applications require knowledge of the behavior of pseudo-plastic fluids within permeable media. For example, enhanced oil recovery processes in naturally fractured petroleum reservoirs can use polymer solutions in water flooding to increase the amount of recovered oil (Green, D.W., Willhite, G.P. (2018)). Another application uses foam, which appears to be the most promising blocking agent in fractured media for underground energy recovery and waste disposal purposes (Hou, M.Z., Xie, H., Were, P., Eds. (2013)). In biological applications, non-Newtonian fluids with shear-thinning character, such as blood and interstitial fluid, flow through the pores of bone tissue, transporting nutrients to, and carrying waste from, the bone cells. Understanding this circulation might provide insight into a number of clinical problems, as reviewed by Cowin, S.C., Cardoso, L. (2015).

Several theoretical approaches might be employed to study flows through porous media, including multiscale homogenization and volume averaging (nicely discussed and compared by Davit, Y., Bell, C.G, Byrne, H.M., Chapman, L.A.C., Kimpton, L.S., Lang, G.E., Leonard, K.H.L., Oliver, J.M., Pearson, N.C., Shipley, R.J., Waters, S.L., Whiteley, J.P., Wood, B.D., Quintard, M. (2013)), mixture theory (see, e.g., Bedford, A., Drumheller, D.S. (1983)), and pore-network ("bundle of tubes") modeling (see, e.g., Balhoff, M.T., Thompson, K.E. (2006).)

Here we employ homogenization, in a form similar to that described by Mei, C.C., Vernescu, B. (2010) to assess the effect of regular pore-scale structures upon a macroscopic flow. Efforts on non-Newtonian rheologies were initiated by Lions, J.L., Sanchez-Palencia, E. (1981) and Bourgeat, A., Mikelić, A. (1993), with focus on the plastic behavior of Bingham fluids. Later, the theory was applied to power-law and Carreau fluids by Bourgeat, A., Mikelić, A. (1996) and Mikelić, A. (2000); all of these authors emphasized mathematical issues of uniqueness of solutions, bounds, and proofs of convergence, as the shear-rate regimes varied.

Filtration laws for non-Newtonian fluids are, in general, non-local, i.e. microscale and macroscale variables do not decouple, which means

* Corresponding author.
E-mail address: alessandro.bottaro@unige.it (A. Bottaro).

https://doi.org/10.1016/j.advwatres.2020.103658
Received 4 November 2019; Received in revised form 27 May 2020; Accepted 13 June 2020
Available online 16 June 2020

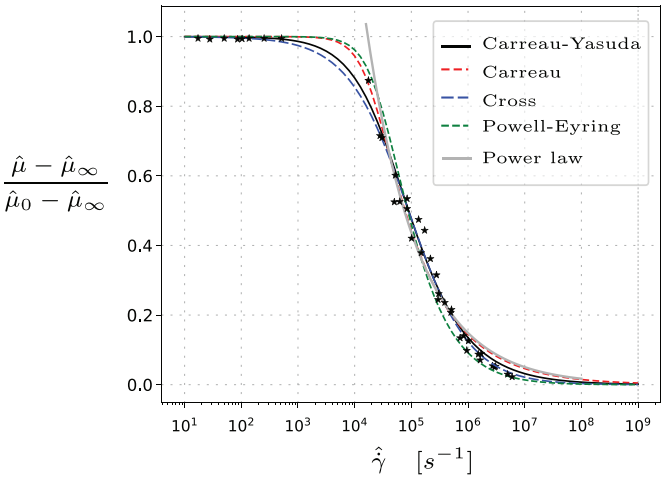

Fig. 1. Rheogram of a shear-thinning fluid. Experimental points by Marx, N., Fernández, L., Barceló, F., Spikes, H. (2018) for the normalized, effective dynamic viscosity $\hat{\mu}$ ($\star$ symbols) are plotted together with the best fits provided by various empirical models. For the case of the power-law model the fit has been done using only the points with $\hat{\dot{\gamma}} > 10^4\,[s^{-1}]$. Notice the Newtonian behavior of the fluid at very high and very low shear rates. For the definition of the axes' labels see later Eq. (5).

that simple microscopic (also called auxiliary) problems capable to yield, upon averaging, an effective permeability tensor for a (macroscopic) Darcy or Darcy-like relation are not available, even when inertia is negligible (Idris, Z., Orgéas, L., Geindreau, C., Bloch, J.-F., Auriault, J.-L. (2004); Orgéas, L., Idris, Z., Geindreau, C., Bloch, J.-F., Auriault, J.-L. (2006); Orgéas, L., Geindreau, C., Auriault, J.-L., Bloch, J.-F. (2007)). For this reason, Götz, T., Parhusip, H.A. (2005) opted to expand the Carreau law in terms of the time constant λ (see later Eq. (5)), assumed small, obtaining a hierarchy of Newtonian-like auxiliary problems, capable to successively approximate the zero-shear-rate solution (for which $\hat{\mu} = \hat{\mu}_0 =$ constant.) With the expansion performed, the solutions decouple and good agreement was found for some selected geometries between the fields computed by direct numerical calculations and those obtained by the asymptotic expansion. We will show later that the limit of small λ yields results which differ very little from the Newtonian case.

One of the alternative upscaling techniques to obtain macroscopic laws is the so-called volume-averaging approach, pioneered by Whitaker, S. (1986); Quintard, M., Whitaker, S. (1993, 1994a, 1994b), and applicable to both organized and disordered porous skeletons. For the case of power-law fluids a generalized Darcy's law is available (cf. Wang, X.-H., Jia, J.-T., Liu, Z.-F., Jin, L.-D. (2014)), with an effective tensorial permeability which can be found from the solution of a problem in a representative elementary volume only once the direction of the average filtration velocity (which, in general, does not coincide with that of the imposed pressure gradient) is prescribed. This is an indication of the strong microscopic-macroscopic coupling; numerical results demonstrate that the components of the effective permeability tensor depend significantly on such a pre-assigned direction. Direct calculations of the pore-scale creeping flow model for a power-law fluid through macroscopic porous media (Zami-Pierre, F., de Loubens, R., Quintard, M., Davit, Y. (2016, 2018)) show that a competition exists between the effect of the non-Newtonian rheology and that related to the order/disorder of the porous structure. In some cases a disordered porous structure might dominate over the non-Newtonian non-linearity, in such a way that the directions of the filtration speed and of the macroscopic pressure gradient are quasi-aligned.

In the simple case of isotropic geometry of the porous medium, the modified Darcy's law which is usually adopted in the engineering community when non-Newtonian fluids are being considered reads (Sadowski, T.J., Bird, R.G. (1965); Christopher, R.H., Middleman, S. (1965); McKinley, R.M., Jahns, H.O., Harris, W.W., Greenkorn, R.A. (1966); Hirasaki, G.J., Pope, G.A. (1974); Shahsavari, S., McKinley, G.H. (2015); Eberhard, U., Seybold, H.J., Floriancic, M., Bertsch, P., Jiménez-Martínez, J., Andrade J.S. Jr., Holzner, M. (2019))

$$\langle \hat{\mathbf{u}}^{(0)} \rangle = -\frac{\hat{\mathcal{K}}}{\hat{\mu}_{\text{eff}}} \hat{\nabla}' \hat{p}^{(0)}, \tag{1}$$

with $\hat{\mathcal{K}}$ the (scalar) Newtonian permeability and $\hat{\mu}_{\text{eff}}$ an *effective viscosity*. The term on the left hand side of Eq. (1) is the average velocity through the porous medium, which is forced by the macroscopic pressure gradient $\hat{\nabla}' \hat{p}^{(0)}$. The crux of the matter is the determination of the effective viscosity which is usually estimated from the rheological law of the fluid for some *effective* value of the shear rate. Engineering practice usually models porous media as a bundle of capillary tubes, as by the approach initiated by Kozeny, J. (1927). When the fluid is non-Newtonian, equating the flow rate of a Newtonian fluid in a straight pipe to that of (say) a power-law fluid yields the power-law viscosity corresponding to the Newtonian viscosity of a fluid which would have produced the same pressure drop along a capillary. Inverting such a law yields an effective shear rate; this is then corrected by the use of empirical parameters to account for the non-uniformity of the medium porosity, the tortuosity of the capillary network, possibly of variable cross-sectional areas, the different orientations of the capillaries, etc. (Sadowski, T.J., Bird, R.G. (1965); Hirasaki, G.J., Pope, G.A. (1974); Cannella, W.J., Huh, C., Seright, R.S. (0000); Berg, S., van Wunnink, J. (2017)). Finally, an effective viscosity is computed from the given constitutive law. An alternative approach to estimate $\hat{\mu}_{\text{eff}}$ for a Carreau fluid has been recently proposed by Eberhard, U., Seybold, H.J., Floriancic, M., Bertsch, P., Jiménez-Martínez, J., Andrade J.S. Jr., Holzner, M. (2019); it is based on a direct solution for the viscosity profile inside a single capillary of given radius, mimicking an average pore through which the mean speed is simply the ratio between Darcy's velocity and the medium porosity. The effective viscosity is then taken to coincide with the volume-averaged viscosity, without the need to introduce and use an effective shear rate. Eberhard et al. also carried out experiments forcing a xanthan gum aqueous solution through a packed of monodisperse beads, finding good agreement between measurements and model results, thus concluding that their *direct* effective viscosity model is a robust approach. Experiments with the same shear thinning fluid, of varying solute concentrations, have also been conducted by Rodriguez de Castro, A., Radilla, G. (2017). They employed Eq. (1) to evaluate the effective viscosity for a Carreau fluid, including the case in which inertial effects are present through the pores, and found a good fits of the data with both Forchheimer's and Ergun's model equations.

Despite its simplicity, Eq. (1) is not supported by either a multiscale nor a volume averaging analysis; also, the equation assumes that the vectors $\langle \hat{\mathbf{u}}^{(0)} \rangle$ and $\hat{\nabla}' \hat{p}^{(0)}$ are parallel, which has been shown to be not necessarily true in several non-Newtonian flow configurations (Idris, Z., Orgéas, L., Geindreau, C., Bloch, J.-F., Auriault, J.-L. (2004); Orgéas, L., Idris, Z., Geindreau, C., Bloch, J.-F., Auriault, J.-L. (2006); Wang, X.-H., Jia, J.-T., Liu, Z.-F., Jin, L.-D. (2014)). We have thus decided to take a new look at the problem, fully accounting for the coupling between microscopic and macroscopic variables. By using homogenization theory, we will demonstrate that, in the limit of creeping flow through the pores, a Darcy-like equation rules the macroscopic behavior of a non-Newtonian fluid in a porous medium, with an effective permeability tensor which is function of the microscopic motion. A detailed parametric study will highlight how the components of the effective permeability and the tensor anisotropy are modified for the case of a Carreau, shear-thinning fluid in a simple geometrical configuration, in response to variations of the medium porosity, of rheological and flow parameters.

2. Formulation of the problem at the pore scale

The equations describing the motion of an incompressible, shear-thinning fluid which saturates the interstices of a porous material read:

$$\rho\left(\frac{\partial \hat{\mathbf{u}}}{\partial \hat{t}} + \hat{\mathbf{u}}\cdot\hat{\nabla}\hat{\mathbf{u}}\right) = -\hat{\nabla}\hat{p} + \hat{\nabla}\cdot[2\hat{\mu}(\hat{\dot{\gamma}})\hat{D}(\hat{\mathbf{u}})], \qquad \hat{\nabla}\cdot\hat{\mathbf{u}} = 0, \tag{2}$$

with $\hat{\mathbf{u}}$ and $\hat{p}$ the dimensional velocity vector and pressure, function in principle of spatial, $\hat{\mathbf{x}}$, and temporal, $\hat{t}$, coordinates. Body forces are taken to be conservative and are absorbed into the pressure gradient term. The hat over a variable's name is used to indicate that the variable is dimensional. The rate of deformation tensor is defined as

$$\hat{D}(\hat{\mathbf{u}}) = \frac{\hat{\nabla}\hat{\mathbf{u}} + \hat{\nabla}\hat{\mathbf{u}}^T}{2}, \tag{3}$$

(superscript T denoting transpose) and its second invariant is

$$\hat{\dot{\gamma}} = \sqrt{2\hat{D}(\hat{\mathbf{u}}) : \hat{D}(\hat{\mathbf{u}})}, \tag{4}$$

with $\hat{\dot{\gamma}}^2$ proportional to the local rate of viscous dissipation of the kinetic energy. The Carreau model Carreau, 1972, with the viscosity which depends on the second invariant of the rate of strain tensor, is chosen to represent the shear-thinning behavior of the fluid for the following reasons:

- It is widely used to describe the rheological behaviour of pseudo-plastic materials and several phenomenological data are available in the literature;
- It has a sound theoretical basis, stemming from the molecular network theory developed by Lodge Lodge A.S. (1968), and has proven capable of modelling simultaneously simple shear, complex viscosity, stress growth and stress relaxation behaviors.

The dynamic viscosity of the Carreau model is

$$\hat{\mu} = \hat{\mu}_\infty + (\hat{\mu}_0 - \hat{\mu}_\infty)\left[1 + \left(\hat{\lambda}\,\hat{\dot{\gamma}}\right)^2\right]^{\frac{n-1}{2}}, \tag{5}$$

with $\hat{\mu}_\infty$ and $\hat{\mu}_0$, respectively, the infinite- and the zero-shear-rate viscosity coefficients ($\hat{\mu}_\infty \ll \hat{\mu}_0$ Bird, R.B., Armstrong, R.C., Hassager, O. (1987); Tanner, R.I. (2000), so that the former can safely be discarded in later analysis), n is the power-law index, representing the degree of shear-thinning, and $\hat{\lambda}$ is the material relaxation time. The parameters in the Carreau model are typically $0.2 \le n < 1$ and $\mathcal{O}(10^{-1}) < \lambda < \mathcal{O}(10^2)$ Bird, R.B., Armstrong, R.C., Hassager, O. (1987) ($\hat{\lambda}$ is made dimensionless with characteristic length and velocity scales, ℓ and $\mathcal{U}$ in the following). Using Fig. 1 as a reference, when the shear rate is low ($\hat{\dot{\gamma}} \ll \hat{\lambda}^{-1}$) the apparent viscosity is equal to $\hat{\mu}_0$; conversely, it becomes negligible when the shear rate is very large.

At this point the variables are normalized as:

$$\mathbf{u} = \frac{\hat{\mathbf{u}}}{\mathcal{U}}, \quad \mathbf{x} = \frac{\hat{\mathbf{x}}}{\ell}, \quad p = \frac{\hat{p}\,\ell^2}{\hat{\mu}_0\,\mathcal{U}\,L}, \quad t = \frac{\hat{t}\,\mathcal{U}}{\ell}. \tag{6}$$

The speed $\mathcal{U}$ is the magnitude of the seepage velocity within the medium and the length ℓ is a characteristic microscopic dimension (e.g. the size of the pores or of the solid inclusions); conversely, L is a (large) length scale of the problem, i.e. the distance across which a macroscopic pressure gradient is imposed. It is further assumed that each dependent variable is function of both a microscopic and a macroscopic length scale (the latter defined as $\mathbf{X} = \hat{\mathbf{x}}/L$), and can be expanded as a power series in terms of the small parameter $\epsilon = \ell/L$ as:

$$f = f^{(0)} + \epsilon f^{(1)} + \epsilon^2 f^{(2)} + \dots, \tag{7}$$

with $f = f(\mathbf{x}, \mathbf{X}, t)$ a generic variable. A multiple scale analysis along the lines of Mei, C.C., Vernescu, B. (2010) leads to finding that, for slow flow through small pores, i.e. when the microscopic Reynolds number, $Re = \rho\,\mathcal{U}\,\ell/\hat{\mu}_0$, is of order ϵ (or smaller), the leading order dimensionless system reduces to

$$-\boldsymbol{\nabla} p^{(1)} + \boldsymbol{\nabla}\cdot[2\mu^{(0)} D(\mathbf{u}^{(0)})] - \nabla' p^{(0)} = 0, \qquad \boldsymbol{\nabla}\cdot\mathbf{u}^{(0)} = 0, \tag{8}$$

with

$$\mu^{(0)} = \mu(\dot{\gamma}^{(0)}) = \left[1 + (\lambda\dot{\gamma}^{(0)})^2\right]^{\frac{n-1}{2}}. \tag{9}$$

System (8) is the same as that given by Orgéas, L., Geindreau, C., Auriault, J.-L., Bloch, J.-F. (2007). The microscopic field ($\mathbf{u}^{(0)}$, $p^{(1)}$) is forced by the imposed, macroscopic pressure gradient, $\nabla' p^{(0)}$. In three-dimensional cartesian coordinates the operator ∇' is $\nabla' = (\partial/\partial X, \partial/\partial Y, \partial/\partial Z)$. The pressure at leading order, also called *pore pressure* or *mean interstitial pressure*, does not depend on microscopic spatial variables. The pressure at order one, $p^{(1)}$, is defined up to an integration "constant" (which is function of only macroscopic spatial variables). In a numerical resolution approach such a constant is set by fixing equal to zero the mean value of $p^{(1)}$ in the fluid domain. The whole domain coincides with the *unit cell* Mei, C.C., Vernescu, B. (2010) in most of the calculations presented in the paper; we assume periodicity of the variables on opposing lateral boundaries of the cell and no-slip at the fluid-solid interface. An example of two-dimensional unit cell is provided in Fig. 2, highlighting the finite element grid used in the computations capable to yield grid-resolved results, and displaying the symmetric isolines of the $u^{(0)}$ and $v^{(0)}$ velocity components, obtained for $(\partial p^{(0)}/\partial X, \partial p^{(0)}/\partial Y) = (1, 0)$ when the fluid is Newtonian ($n = 1$); the physical set up of Fig. 2 has a porosity equal to $\theta = \mathcal{V}_{\text{fluid}}/\mathcal{V}_{\text{tot}} = 0.90$, with $\mathcal{V}_{\text{fluid}}$ the volume occupied by the fluid and $\mathcal{V}_{\text{tot}}$ the total volume of the unit cell (fluid plus solid).

3. Adjoint homogenization: Darcy's equation and the non-Newtonian permeability

To derive the macroscopic equation ruling the motion of a non-Newtonian fluid in a porous medium formed by periodic repetitions of unit cells we follow the adjoint homogenization approach outlined by Bottaro, A. (2019), forming the dot product of system (8) with the test vector ($\mathbf{u}\dagger$, $p\dagger$), and integrating over the fluid domain. Integrations by parts are then conducted, employing the periodicity conditions on the outer boundaries of the domain and the no-slip condition on the grain's boundary, to identify the adjoint system which holds in the unit cell:

$$-\boldsymbol{\nabla} p^\dagger + \boldsymbol{\nabla}\cdot[2\mu^{(0)} D(\mathbf{u}^\dagger)] = -\mathbf{G}, \qquad \boldsymbol{\nabla}\cdot\mathbf{u}^\dagger = 0, \tag{10}$$

with the vector $\mathbf{G}$ defined below. Problem (10) must satisfy conditions of periodicity for $\mathbf{u}\dagger$ and $p\dagger$ on the lateral boundaries of the unit cell, plus $\mathbf{u}^\dagger = \mathbf{0}$ on the boundaries of the solid inclusions. For uniqueness of the adjoint state we also impose the vanishing of the integral of $p\dagger$ over $\mathcal{V}_{fluid}$. The coupling of direct and dual problems, via the fluid viscosity $\mu^{(0)}$ evaluated from the leading order velocity, is inevitably due to the non-linearity of the direct system (8).

With systems (8) and (10) (and respective boundary conditions) posed as above, the Lagrange-Green identity readily yields:

$$\int_{\mathcal{V}_{\text{fluid}}} \left(\mathbf{G}\cdot\mathbf{u}^{(0)} + \mathbf{u}^\dagger\cdot\nabla' p^{(0)}\right) \mathrm{d}\mathcal{V} = 0. \tag{11}$$

We now divide Eq. (11) by the total volume of the unit cell, to obtain

$$\langle \mathbf{G}\cdot\mathbf{u}^{(0)}\rangle = -\langle \mathbf{u}^\dagger\rangle\cdot\nabla' p^{(0)}. \tag{12}$$

where

$$\langle a\rangle = \frac{1}{\mathcal{V}_{\text{tot}}}\int_{\mathcal{V}_{\text{fluid}}} a\,\mathrm{d}\mathcal{V} \tag{13}$$

denotes the *phase*, or *superficial, average* of the generic quantity a. For simplicity of notation, we switch to two-dimensional cartesian coordinates, and set up the two auxiliary problems which follow:

- *Problem 1* Set $\mathbf{G} = (1, 0)$ and solve system (10). Eq. (12) then yields the horizontal component of the seepage velocity:

$$\langle u^{(0)}\rangle = -\mathcal{K}^C_{xx}\frac{\partial p^{(0)}}{\partial X} - \mathcal{K}^C_{xy}\frac{\partial p^{(0)}}{\partial Y}, \tag{14}$$

with $\mathcal{K}^C_{xx} = \langle u^{\dagger(1)}\rangle$ and $\mathcal{K}^C_{xy} = \langle v^{\dagger(1)}\rangle$. Superscript (1) (or (2)) next to the dagger in the name of the adjoint variables is used to indicate

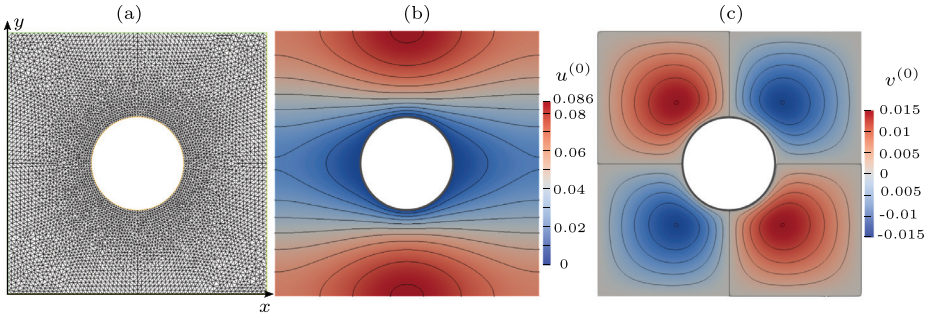

Fig. 2. Two-dimensional, periodic unit cell with the solid, circular inclusion shown in white color. The image labelled (a) shows the grid used for the computations, composed by 10 808 triangles; Newtonian results for $\mathbf{F} = (1, 0)$ are displayed in frames (b) and (c), via isolines of, respectively, horizontal (x-aligned) and vertical (y-aligned) velocity components.

the solution of problem 1 (or 2). Eq. (14) defines two components of the effective permeability tensor $\mathbf{K}^C$.

- *Problem 2* Set $\mathbf{G} = (0, 1)$ for Eq. (12) to yield the vertical component of the seepage velocity:

$$\langle v^{(0)} \rangle = -\mathcal{K}^C_{yx} \frac{\partial p^{(0)}}{\partial X} - \mathcal{K}^C_{yy} \frac{\partial p^{(0)}}{\partial Y}, \tag{15}$$

with the two other permeability components $\mathcal{K}^C_{yx} = \langle u^{\dagger(2)} \rangle$ and $\mathcal{K}^C_{yy} = \langle v^{\dagger(2)} \rangle$.

It needs to be stressed that the four components of the tensor $\mathbf{K}^C$ are available after solving the linear system (10) twice in the microscopic unit cell. The extension to three dimensions is trivial and will not be pursued here, the present contribution being limited to illustrating two-dimensional results.

The dimensionless Darcy's law is thus recovered, and in compact form it reads

$$\langle \mathbf{u}^{(0)} \rangle = -\mathbf{K}^C \cdot \nabla' p^{(0)}. \tag{16}$$

This equation relates the Darcy's velocity of a pseudo-plastic fluid in a porous medium to the macroscopic gradient of the pore pressure via a Carreau permeability tensor, $\mathbf{K}^C$, also called the *effective mobility tensor* Shahsavari, S., McKinley, G.H. (2015), which depends on the direct flow state through $\dot{\gamma}^{(0)}$, so that macroscopic and microscopic state variables do not decouple. The vector Eq. (16) must be solved together with the mass-conservation constraint which, by virtue of the spatial-averaging theorem Mei, C.C., Vernescu, B. (2010), is simply $\nabla' \cdot \langle \mathbf{u}^{(0)} \rangle = 0$.

In dimensional form, the effective Darcy's Eq. (16) reads:

$$\langle \hat{\mathbf{u}}^{(0)} \rangle = -\frac{1}{\hat{\mu}_0} \hat{\mathbf{K}}^C \cdot \hat{\nabla}' \hat{p}^{(0)}, \tag{17}$$

with $\hat{\mathbf{K}}^C = \mathbf{K}^C \ell^2$. Using the Newtonian (or intrinsic) permeability $\hat{\mathbf{K}}$, Eq. (17) takes the alternative form

$$\langle \hat{\mathbf{u}}^{(0)} \rangle = -\frac{1}{\hat{\mu}_0} \mathbf{\Phi} \cdot \hat{\mathbf{K}} \cdot \hat{\nabla}' \hat{p}^{(0)}, \tag{18}$$

with $\mathbf{\Phi} = \hat{\mathbf{K}}^C \cdot \hat{\mathbf{K}}^{-1}$, whose dimensionless version is simply

$$\langle \mathbf{u}^{(0)} \rangle = -\mathbf{\Phi} \cdot \mathbf{K} \cdot \nabla' p^{(0)}. \tag{19}$$

Eq. (18) is the extended version of Eq. (1) in which $\mathbf{\Phi}/\hat{\mu}_0$ plays the role of a *fluidity tensor*McCain Jr., W.D. (1990). The simplest possible form of this tensor is, in principle, $\mathbf{\Phi}/\hat{\mu}_0 = \phi\, \mathbf{I}/\hat{\mu}_0$ ($\mathbf{I}$ being the identity matrix), with the *effective viscosity* which would thus become $\mu_{\text{eff}} = \hat{\mu}_{\text{eff}}/\hat{\mu}_0 = 1/\phi$ (cf. Eq. (1)). For the isotropic geometry displayed in Fig. 2 it is $\mathbf{K} = \mathcal{K}\, \mathbf{I}$, so that $\mathbf{\Phi}$ coincides with the Carreau permeability up to the multiplicative constant $\mathcal{K}^{-1}$. However, even for the elementary isotropic arrangement of solid inclusions under consideration here, $\mathbf{\Phi}$ does **not** take the simple form $\mathbf{\Phi} = \phi\, \mathbf{I}$ (and, likewise, we cannot write $\mathbf{K}^C = \mathcal{K}^C\, \mathbf{I}$), so that, aside from limiting cases in which deviations from the Newtonian behavior are minimal, it is not formally correct to introduce an *effective viscosity* and use Darcy's law together with a scalar, Newtonian permeability. This conclusion, to be supported shortly by numerical results, is a major departure from standard engineering practice. We also observe that Eq. (18) has been *postulated* recently by Zami-Pierre, F., de Loubens, R., Quintard, M., Davit, Y. (2018), and $\mathbf{\Phi}$ was interpreted as the product of a rotation tensor, to capture changes in the direction of the average velocity with respect to the Newtonian case, times a scalar factor capable to account for variations in velocity magnitude because of non-Newtonian effects.

The aim of this paper is to assess and discuss, for the geometry of Fig. 2, variations of the Carreau permeability with the fluid properties, λ and n, with the porosity of the medium, θ, and with the orientation of the macroscopic, forcing pressure gradient. The norm of $\nabla' p^{(0)}$ will, from now on, be taken unitary, and the pressure gradient parameterized by the angle $\alpha \in [0°, 90°]$, i.e.

$$\frac{\partial p^{(0)}}{\partial X} = -\cos\alpha, \quad \frac{\partial p^{(0)}}{\partial Y} = -\sin\alpha. \tag{20}$$

The limiting cases $\alpha = 0°$ and $\alpha = 90°$ correspond to pressure gradient along X and Y, respectively, with the fluid being forced from left to right in the first case and from bottom to top in the second, with reference to the axes in Fig. 2. Results for other macroscopic forcing directions can easily be recovered by rotation.

4. Numerical method, validation and sample results

The incompressible two-dimensional creeping flow Eq. (8) are solved with a finite element method using the FreeFEM open source code Hecht, F. (2012). The approach is based on a weak formulation of the equations, which means introducing two regular test functions q and $\mathbf{v}$, and solving the integral

$$\int_{\mathcal{V}_{\text{fluid}}} (-2\,\mu(\dot{\gamma}^{(0)})\, D\mathbf{u}^{(0)} \cdot \nabla \mathbf{v} + q\, \nabla \cdot \mathbf{u}^{(0)} + p^{(1)}\, \nabla \cdot \mathbf{v} - \nabla' p^{(0)} \cdot \mathbf{v})\, d\mathcal{V} = 0 \tag{21}$$

for the direct variables $p^{(1)}$ and $\mathbf{u}^{(0)}$, approximated by triangular $P_1 - P_2$ Taylor-Hood elements Brezzi, F., Falk, R. (1991); Chen, L. (2014). The non-linearity present in the viscosity law is treated by the use of the Newton method, and a few iterations (typically between four and ten) are needed to obtain a converged solution for the direct flow state. A similar approach in weak form is also employed for the $\mathbf{u}^{(0)}$-dependent adjoint problem.

The mesh, $n_s \times n_c$, is defined by the number of points n_s, equi-distributed along each side of the square computational box, and the number of points n_c, equi-distributed on the boundary of the circular solid inclusion. Numerical results have been obtained with three grids: 60×120, 120×180 and 200×360. For $\theta = 0.9$ these yield, respectively, 10 808, 36 378 and 111 516 triangles. The results obtained with the fine mesh (mesh 3) are used as a reference against which to measure the results obtained with the coarser grids. In particular, a percentage error sensor on the permeability (whether intrinsic or non-Newtonian) can be defined, as

$$e_i(\mathcal{K}^C_{xx}) = \frac{|(\mathcal{K}^C_{xx})_i - (\mathcal{K}^C_{xx})_3|}{(\mathcal{K}^C_{xx})_3}, \quad i = 1 \text{ and } 2, \tag{22}$$

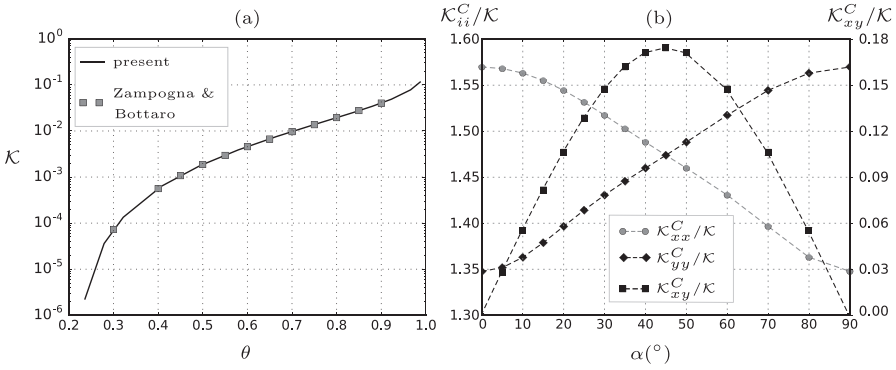

Fig. 3. (a) Intrinsic permeability against porosity for a regular arrangement of circulardisks. (b) Components of the apparent permeability tensor of a Carreau fluid (normalized by $\mathcal{K} = 0.0403$) for varying directions of the mean pressure gradient ($\theta = 0.9$, $n = 0.5$, $\lambda = 5$).

Table 1
Mesh convergence analysis for Newtonian and Carreau fluid in terms of the components of the permeability tensor (in the Carreau case we have selected $n = 0.5$ and $\lambda = 5$, while in the Newtonian case it is simply $n = 1$). The matrix porosity is $\theta = 0.9$ and the driving pressure gradient is parallel to the x-axis (i.e. $\alpha = 0°$). For such a forcing condition it is $\mathcal{K}^C_{xy} = \mathcal{K}^C_{yx} = 0$ for both rheologies.

	$\mathcal{K}^C_{xx}$	$\mathcal{K}^C_{yy}$	$e_1(\mathcal{K}^C_{xx})$	$e_1(\mathcal{K}^C_{yy})$	$e_2(\mathcal{K}^C_{xx})$	$e_2(\mathcal{K}^C_{yy})$
Newtonian	0.0403	0.0403	0.030%	0.030%	0.010%	0.010%
Carreau	0.0632	0.0543	0.040%	0.040%	0.015%	0.015%

Table 2
Effective, anisotropic components of the permeability for the case of Fig. 4, against the single permeability component which arises when introducing an effective viscosity.

$\mathcal{K}^C_{xx}$	$\mathcal{K}^C_{yy}$	$\mathcal{K}^C_{xy}$	μ_{eff}	$\mathcal{K}/\mu_{\text{eff}}$
			0.5315	0.0758
0.1034	0.0962	0.0162	0.4505	0.0894

and likewise for $\mathcal{K}^C_{yy}$. The subscript 1, 2 or 3 next to the permeability component indicates that the component is evaluated on the basis of grid 1, 2 or 3 (1 being the coarsest). Thus, for example, $e_1(\mathcal{K}^C_{xx})$ represents the percentage difference between the values of the streamwise permeability component obtained with grids 1 and 3. Representative results for both the Newtonian and a Carreau rheology are reported in Table 1 and are very reassuring in terms of the accuracy of the numerical procedure; for example, grid 1 yields values of $\mathcal{K}^C_{xx}$ and $\mathcal{K}^C_{yy}$ which are always within 0.040% of those obtained with the (very fine) grid 3. Additional information on the grid convergence of the results is provided in Appendix A. In the following, all results reported are obtained using grid 1, which permits a faster and accurate exploration of parameter space.

For a Newtonian fluid, the results obtained with grid 1 coincide to graphical accuracy with those reported previously by Zampogna, G., Bottaro, A. (2016), as shown in Fig. 3(a).

For the same non-Newtonian parameters as used in Table 1, it is instructive to study how the effective permeability components change with the variation of the angle α of the forcing pressure gradient. These results are reported in Fig. 3(b) and highlight the symmetry of the problem; in particular, $\mathcal{K}^C_{xx}(\alpha) = \mathcal{K}^C_{yy}(90° - \alpha)$, $\mathcal{K}^C_{xy}(\alpha) = \mathcal{K}^C_{xy}(90° - \alpha)$ and $\mathcal{K}^C_{xy} = \mathcal{K}^C_{yx}$. The off-diagonal components of the permeability are typically one order of magnitude smaller that the diagonal components, but cannot be neglected. Their maximum values are found when the pressure gradient is oriented at 45° with respect to the horizontal (or at 135°). For these two angles, it is also $\mathcal{K}^C_{xx} = \mathcal{K}^C_{yy}$ as clearly imposed by symmetry.

It is also instructive to focus on microscopic results in a non-Newtonian case, to try and assess how the viscosity varies within the unit cell, via its coupling with the strain, and to evaluate whether an *effective viscosity* can be introduced. Fig. 4 displays direct microscopic solutions computed for a Carreau fluid with $n = 0.5$ and $\lambda = 10$, with the porosity of the regular arrangement of disks maintained at $\theta = 0.9$, and the macroscopic pressure gradient oriented at $\alpha = 30°$. In Fig. 4(a) the focus is on the second invariant of the rate of deformation tensor; the image demonstrates the presence of strongly deformed, localized regions of the flow, sitting next to other regions characterized by very low values of $\dot{\gamma}^{(0)}$.

This behavior reflects directly onto the distribution of viscosity, shown in Fig. 4(b). A large apparent viscosity is present in areas where $\dot{\gamma}^{(0)}$ is low, and viceversa. From these results it is easy to extract, via *intrinsic averaging*, the mean viscosity and the mean strain. In particular, denoting the intrinsinc averaging operation Whitaker, S. (1986) with $\langle \cdot \rangle^f$ we have:

$$\langle \mu^{(0)} \rangle^f = \frac{1}{\mathcal{V}_{\text{fluid}}} \int_{\mathcal{V}_{\text{fluid}}} \mu^{(0)} \, \mathrm{d}\mathcal{V} = \frac{1}{\theta} \langle \mu^{(0)} \rangle = 0.5315, \tag{23}$$

$$\langle \dot{\gamma}^{(0)} \rangle^f = \frac{1}{\mathcal{V}_{\text{fluid}}} \int_{\mathcal{V}_{\text{fluid}}} \dot{\gamma}^{(0)} \, \mathrm{d}\mathcal{V} = 0.4825. \tag{24}$$

The latter averaged value can be introduced into the viscosity law (9) to yield another estimate of the dimensionless *effective viscosity*, $\mu_{\text{eff}} = 0.4505$. Whether one uses 0.4505 (as suggested, for example, by Shahsavari & McKinley Shahsavari, S., McKinley, G.H. (2015)) or avoids going through the strain rate and uses directly the intrinsic average value 0.5315 (as suggested by Eberhard, U., Seybold, H.J., Floriancic, M., Bertsch, P., Jiménez-Martínez, J., Andrade J.S. Jr., Holzner, M. (2019)) the conclusion is the same and is readily apparent through inspection of the numbers in Table 2. An effective viscosity method is incapable of accounting for anisotropic effects and underestimates the permeability to be used in Eq. (16). This is also clear after evaluating the eigenvalues of $\mathbf{K}^C$ which, in this case, are equal to $\lambda_{\max} = 0.1164$ and $\lambda_{\min} = 0.0832$; the anisotropy factor, defined as

$$\delta = \frac{\lambda_{\max}}{\lambda_{\min}}, \tag{25}$$

is appreciably larger than one ($\delta = 1.399$) and the mean permeability, geometric average of the principal permeabilities, is $\mathcal{K}_{\text{mean}} = \sqrt{\lambda_{\max} \lambda_{\min}} = 0.0984$, exceeding by 14% the largest value of $\mathcal{K}/\mu_{\text{eff}}$ in Table 2.

The components of the effective mobility tensor, $\mathcal{K}^C_{ij}$, in Table 2 are obtained by phase averaging adjoint "velocities", as defined right after Eqs. (14) and (15). Such microscopic adjoint fields, for the geometry and the fluid being discussed here, are shown in Fig. 5. Whereas the two fields $v^{\dagger(1)}$ and $u^{\dagger(2)}$ are the same, aside from a 90° rotation plus reflection operation, the two fields which yield the diagonal components of $\mathbf{K}^C$, after rotation and reflection, still display some differences (and, in fact, $\mathcal{K}^C_{xx}$ is about 7% larger than $\mathcal{K}^C_{yy}$.)

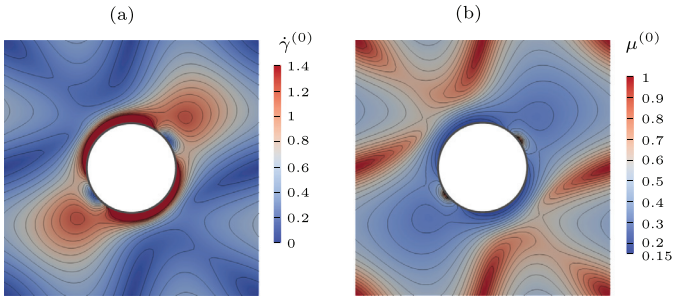

Fig. 4. (a) Second invariant of the rate of strain tensor, $\dot{\gamma}^{(0)}$, and (b) viscosity $\mu^{(0)}$. The macroscopic pressure gradient within the unit cell is inclined at $\alpha = 30°$ with respect to the direction of the x-axis.

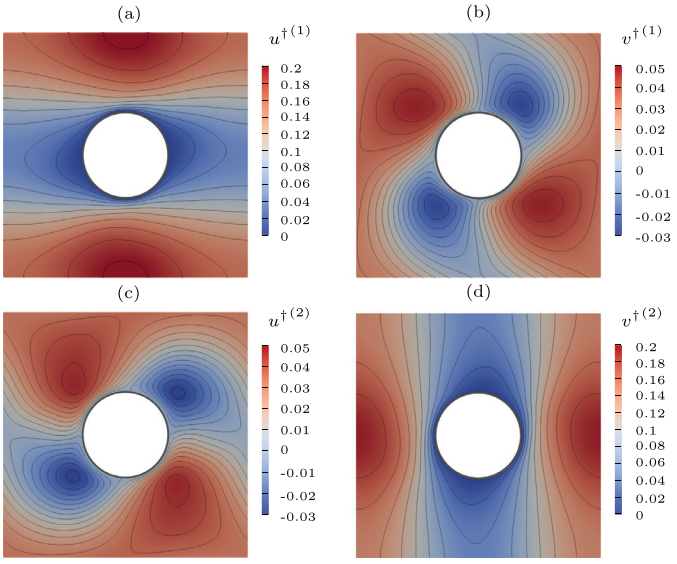

Fig. 5. Adjoint fields for the microscopic problems defined, respectively, by $\mathbf{G} = (1, 0)$ (superscript (1)) and $\mathbf{G} = (0, 1)$ (superscript (2)) for the same Carreau fluid as in Fig. 4.

5. Parametric analysis

The main output of the parametric study is the apparent permeability tensor, with its three independent components, $\mathcal{K}^C_{xx}$, $\mathcal{K}^C_{yy}$ and $\mathcal{K}^C_{xy}$; another interesting output is the anisotropy factor, δ, which stems directly from the mobility tensor. Four input variables are present; one of them, α, is related to the orientation of the macroscopic pressure gradient, another is the porosity θ of the medium, and the last two, n and λ, are related to rheological properties of the fluid. The space of parameters is thus formidable and here we aim to provide a reasonably complete and accurate synthesis of the results, based on over 3 300 direct-adjoint numerical simulations.

5.1. Trend of the viscosity with carreau parameters

First, it is instructive to assess how the viscosity changes with the Carreau parameters n and λ, since the more the fluid's behavior differs from Newtonian, the more anisotropic we expect the permeability tensor to be. We have thus fixed the value of the second invariant of the rate of strain tensor to a (reasonable) constant value, i.e. $\dot{\gamma}^{(0)} = 0.5$ (cf. Fig. 4(a)); a different choice of the value of $\dot{\gamma}^{(0)}$ does not change the qualitative trend of $\mu^{(0)}$ which can be observed in Fig. 6. For small λ the fluid acts as Newtonian (in the case being consider the upper threshold is about $\lambda = 1$); the behavior of $\mu^{(0)}$ with n in the limit $\lambda\dot{\gamma}^{(0)} \to 0$ is

$$\mu^{(0)} \approx 1 + \frac{n-1}{2}[\lambda\,\dot{\gamma}^{(0)}]^2 + \frac{(n-1)(n-3)}{8}[\lambda\,\dot{\gamma}^{(0)}]^4. \tag{26}$$

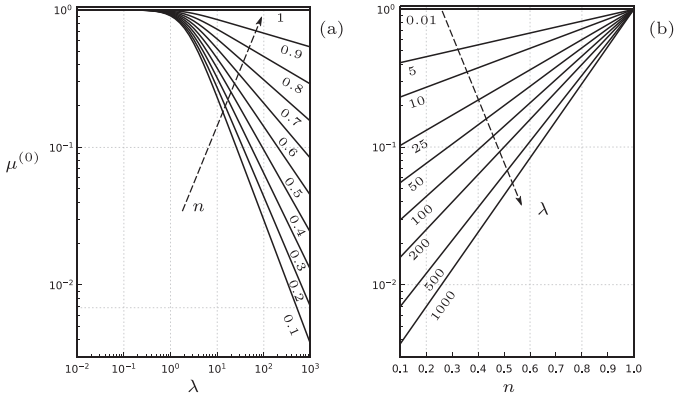

Fig. 6. Carreau viscosity $\mu^{(0)}$ for $\dot{\gamma}^{(0)}$ fixed at 0.5. Variation of $\mu^{(0)}$ versus λ (a) and versus n (b). Arrows indicate increasing values of the parameters n (in frame a) and λ (b).

With the increase of λ (above a few units) the typical Ostwald-de Waele Ostwald, W. (1929) power-law relationship ensues, of the form

$$\mu^{(0)} \approx [\lambda\,\dot{\gamma}^{(0)}]^{n-1}, \tag{27}$$

with λ^{n-1} the dimensionless flow consistency index. The trends expressed by Eqs. (26) and (27) are represented in Fig. 6(a). The variation of the viscosity with n is more clearly displayed in frame (b) of the same figure. When $n = 1$ the fluid is Newtonian for any λ, and $\mu^{(0)} = 1$; a mild deviation from $n = 1$ yields

$$\mu^{(0)} \approx 1 - \frac{1-n}{2}\,\ln\left\{1 + [\lambda\,\dot{\gamma}^{(0)}]^2\right\}. \tag{28}$$

As n is reduced further the fluid becomes more shear-thinning and when $n \to 0$ the asymptotic behavior is

$$\mu^{(0)} \approx \left\{1 + \frac{n}{2}\,\ln[1 + (\lambda\dot{\gamma}^{(0)})^2]\right\}\left\{1 + [\lambda\dot{\gamma}^{(0)}]^2\right\}^{-\frac{1}{2}}, \tag{29}$$

with $\mu^{(0)}$ which decreases more rapidly with the increase of $\lambda\dot{\gamma}^{(0)}$.

The observations just made reflect onto the components of the Carreau permability. In particular, we will verify that the normalized components of the effective mobility tensor, $\tilde{\mathcal{K}}_{xx} = \mathcal{K}^C_{xx}/\mathcal{K}$ and $\tilde{\mathcal{K}}_{yy} = \mathcal{K}^C_{yy}/\mathcal{K}$ (thus, scaled by the intrinsic permeability $\mathcal{K}$, evaluated at the same value of the porosity, θ) tend to 1 in the limit of λ going to 0 or n to 1. We will further show that the off-diagonal, normalized permeability term, $\tilde{\mathcal{K}}_{xy} = \mathcal{K}^C_{xy}/\mathcal{K}$, approaches zero in the same limits. Finally, when λ becomes very large, the Carreau viscosity model reverts to the simpler power-law equation.

5.2. The normalized permeability

Because of the property $\mathcal{K}^C_{xx}(45° - \Delta\alpha) = \mathcal{K}^C_{yy}(45° + \Delta\alpha)$ (cf. Fig. 3(b)) only the behavior of the first component of the normalized mobility tensor will be described, with α ranging from 0° to 90°. Values of $\tilde{\mathcal{K}}_{yy}$ are immediately available by symmetry. To analyze the behavior of $\tilde{\mathcal{K}}_{xx}$ we first evaluate it against the relaxation time, λ (cf. Fig. 7) and then against the porosity, θ (cf. Fig. 8). Isotropicity is maintained until λ remains below an order one threshold value, function of the other (flow and rheological) parameters. As the time constant in the Carreau law exceeds the threshold, the permeability grows monotonically, and the more so for increasing porosity, and decreasing power law index and forcing angle. The behavior of the first mobility coefficient against λ (Fig. 7) is remarkably similar to that of $\mu^{(0)}$ sketched in Fig. 6(a) (where $\dot{\gamma}^{(0)}$ had been set, for simplicity, to a constant value), and can be expressed by the following law:

$$\tilde{\mathcal{K}}_{xx} \approx (1 + A\lambda^p)^{\frac{1}{m}}, \tag{30}$$

with m and p positive, real numbers. At each fixed n, it is $m = p$. In general, the coefficients A, m and p depend non-trivially on the parameters of the problem and can be identified by regression analysis.

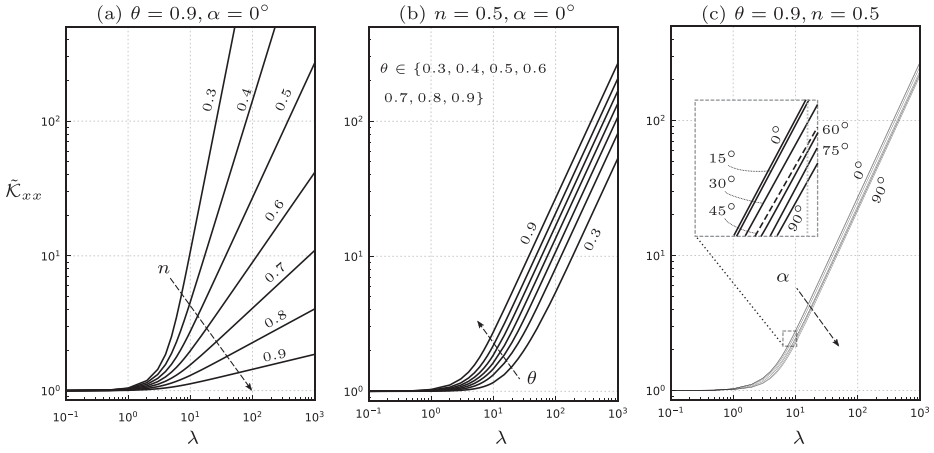

Fig. 7. Variation of $\tilde{\mathcal{K}}_{xx}$ with λ. In frame (a) θ and α are kept constant, equal to the values indicated above the figure, and the different curves are parameterized by n, with n increasing in the direction of the arrow. In frame (b) the curves are parameterized by θ, with n and α constant, while in frame (c) the parameters kept at a fixed value are θ and n, with different lines drawn by varying the angle α.

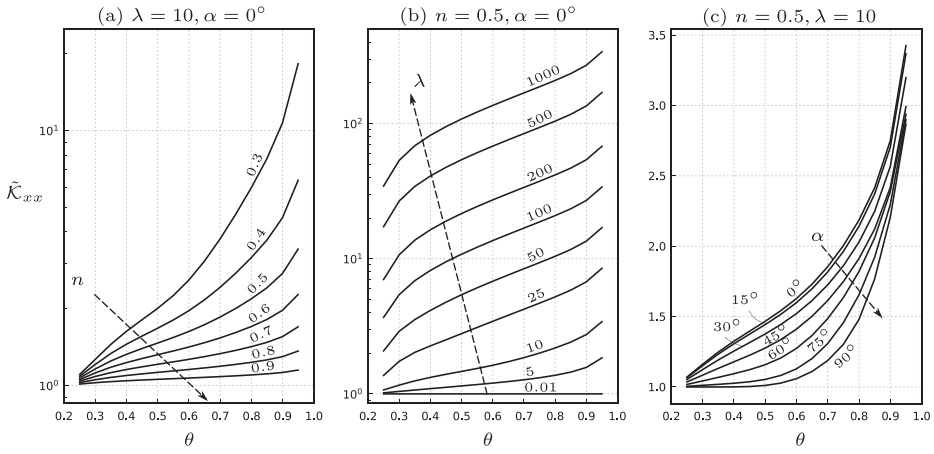

Fig. 8. Variation of $\tilde{\mathcal{K}}_{xx}$ with θ.

When looking at the results in a $\tilde{\mathcal{K}}_{xx}$ versus θ plot, the trends are also monotonic and the role of the parameters discussed on the basis of Fig. 7 is confirmed, cf. Fig. 8. In particular, the shape of all curves is well fit by an expression of the form

$$\tilde{\mathcal{K}}_{xx} \approx \frac{A' \, \theta^{m'}}{(1-\theta)^{p'}}. \tag{31}$$

Interestingly, Eq. (31) has the same form of Kozeny equation Kozeny, J. (1927), aside from the fact that the regression parameters A', m' and p' depend on the constant in the viscosity law and on the direction of the forcing pressure gradient. It is also found that the exponential increase of $\tilde{\mathcal{K}}_{xx}$ with n is well correlated by

$$\ln \tilde{\mathcal{K}}_{xx} \approx \frac{A'' \, (1-n)^{p''}}{n^{m''}}. \tag{32}$$

for any λ, θ and α. As before, the regression coefficients in Eq. (32) depend non-linearly on all other parameters. We have unfortunately been unable to sort out a single equation, $\tilde{\mathcal{K}}_{xx} = f(\theta, \alpha, \lambda, n)$, capable to independently account for the variation of each variable.

The off-diagonal component of the Carreau permeability is symmetric about $\alpha = 45°$ (cf. Fig. 3(b)), which is why in this case the parametric plots cover only the interval of angles from 0° to 45°. The results in Fig. 9 show how $\tilde{\mathcal{K}}_{xy}$ changes with α upon variation of the other parameters. The off-diagonal component of $\mathbf{K}^C$ rises monotonically from zero at $\alpha = 0°$ to a maximum at $\alpha = 45°$, reaching non-negligible magnitudes when compared to those of the diagonal components. Large values of the porosity, θ, and of the time constant, λ, as well as a low power-law index, n, yield increasing $\tilde{\mathcal{K}}_{xy}$, just as it occurs for the diagonal component $\tilde{\mathcal{K}}_{xx}$. Analysis of the plots in Fig. 9 further reveals that as long as α does not exceed about 25°, $\tilde{\mathcal{K}}_{xy}$ depends linearly on α, i.e.

$$\tilde{\mathcal{K}}_{xy} \approx C(\theta, n, \lambda)\, \alpha, \tag{33}$$

with the slope coefficient a non-trivial function of the other parameters. Furthermore, by considering a figure analogous to Fig. 9(b), but with λ in abscissa and α as a parameter, an accurate power law regression yields an expression of the form:

$$\tilde{\mathcal{K}}_{xy} \approx \frac{\tilde{A} \, \lambda^{\tilde{p}}}{(1 + \tilde{B}\lambda^{\tilde{q}})^{\frac{1}{\tilde{m}}}}, \tag{34}$$

with coefficients, $\tilde{A}$ and $\tilde{B}$, and exponents, $\tilde{p}$, $\tilde{q}$ and $\tilde{m}$, functions of the other parameters; in particular, $\tilde{q}$ is close to $\tilde{m}$ and $\tilde{p}$ is quasi-constant and equal to 2 in this situation ($n = 0.5$, $\theta = 0.9$).

The results obtained attest to the strong non-linear footprint of Carreau's rheology on the fluid flow and on the effective quantities appearing in Darcy's equation.

5.3. The anisotropy factor

A concise way to sum up the results of the parametric study is allowed by focusing on the anisotropy factor. Fig. 10 displays δ as function of the dimensionless relaxation time λ. The immediate observation is that the permeability is a scalar quantity (isotropic conditions) at low λ's (as already seen before, when λ is less than about 1, Newtonian conditions are recovered). The anisotropy factor then rises monotonically in some range of λ, range which stretches with the increase of α and the decrease of θ. Conversely, the interval of values of λ over which δ grows appears to be independent of the power-law index, n. After this region of growth, the anisotropy factor saturates. Larger values of δ are

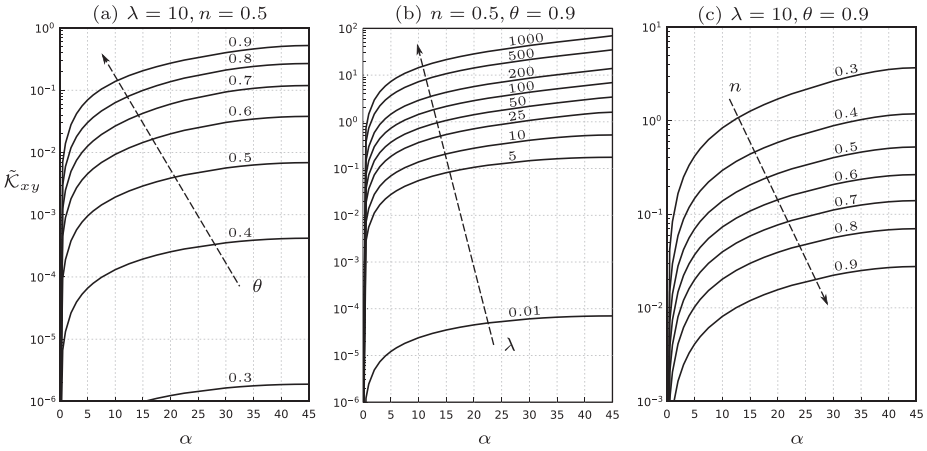

Fig. 9. Parametric variation of $\tilde{\mathcal{K}}_{xy}$ as function of α (expressed in degrees).

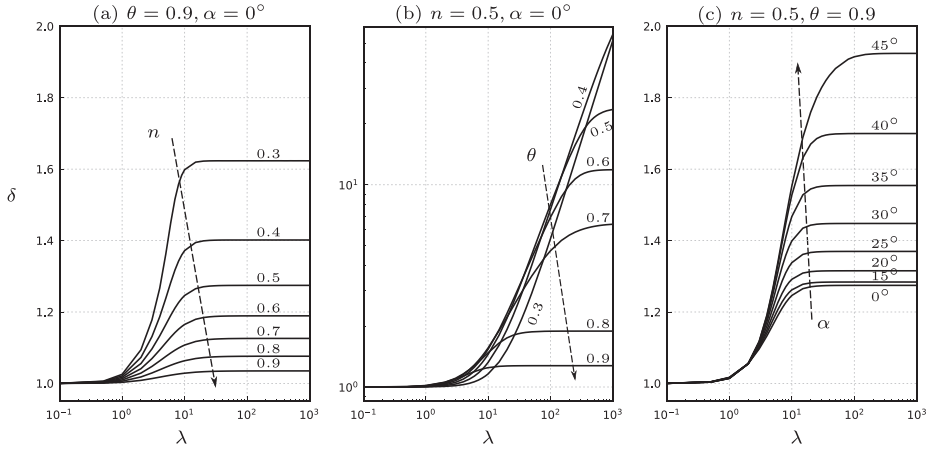

Fig. 10. Variation of anisotropy factor with λ.

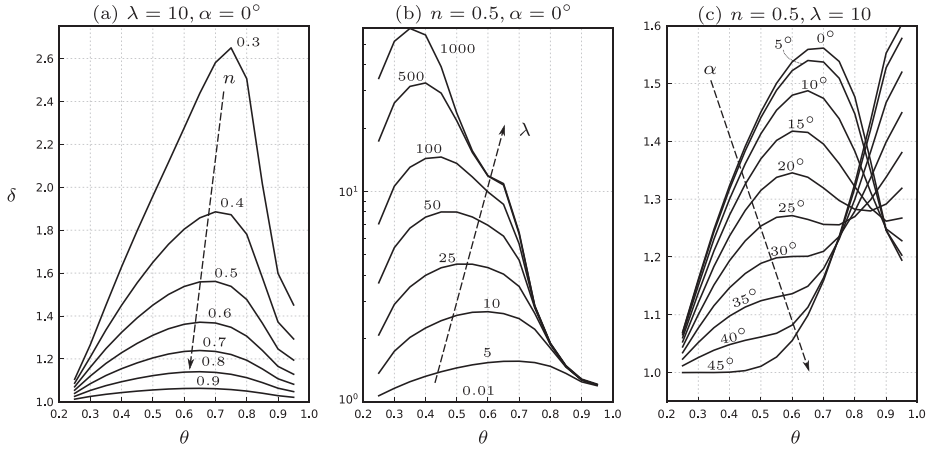

Fig. 11. Variation of anisotropy factor with θ.

observed for $\alpha = 45°$, when the porosity is small and for low n's. In the limit of very small n, the viscosity is ruled by Eq. (29) and $\mu^{(0)}$ tends to zero when $\lambda\dot{\gamma}^{(0)} \to +\infty$. Thus, as λ increases and n decreases, the permeability tensor becomes more anisotropic and, as anticipated, this is associated to a reduced value of the fluid's dynamic viscosity.

Fig. 10 seems to suggest that the anisotropy factor can only grow monotonically with λ, and more so for larger α's, but this is the case only when the porosity is large ($\theta = 0.9$ in Fig. 10(b).) An alternative manner to observe the system's behavior is displayed in Fig. 11, where δ is plotted against the porosity.

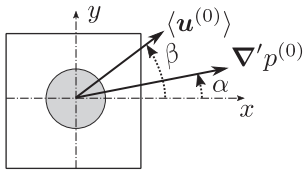

Fig. 12. The flow angles.

The figure indicates clearly that δ does not behave monotonically with θ. In particular, the system is more anisotropic for θ in a range around 0.7 when α and λ are fixed as in frame (a); the maximum value of δ shifts to lower porosities as the relaxation time λ grows (frame b). Frame (c) of Fig. 11 illustrates the behavior of δ with the angle of the imposed pressure gradient. At low α's (until about 15° for the chosen λ and n) there is a peak at an intermediate value of porosity; when α exceeds an angle of about 20° the most anisotropic configurations are found when the porosity tends to its upper limit value ($\theta \to 1$), i.e. for solid grains of small size. In other words, when the pores are small the largest anisotropy occurs at $\alpha = 0$; when the pores become sufficiently large the maximum δ occurs when the angle between the axes and the pressure gradient is 45°. This behavior highlights the non-trivial influence of porosity and inclination of the pressure forcing on the strain field and, as a consequence, on the system's anisotropic response.

5.4. Flow angles

Another aspect linked to the anisotropicity of this system is the angle between the directions of the mean flow velocity vector, $\langle \mathbf{u}^{(0)} \rangle$, and of the macroscopic pressure gradient, $\nabla' p^{(0)}$. Such an angle is defined in Fig. 12, as the difference between β and α. The deviation angle varies with the parameters of the problem as displayed in Fig. 13.

Coherently with the indications of the previous section, $\beta - \alpha$, hence the system's anisotropy, is enhanced by increasing values of λ, with a saturation observed for λ exceeding a value of about 25, and decreasing values of n; not unexpectedly, the behavior with θ is not monotonic. On the positive side, the deviation angle remains always limited to a few degrees and this bodes well for the development of simplified models.

5.5. Effects of flow domain's size and grains' randomness

The final point which deserves scrutiny is the effect of the domain's size. Until now all results have concerned the case of a single unit cell. However, the nonlinearity of the direct problem suggests asking (and trying to answer) the question: is the single unit cell a sufficient domain for this analysis? A related question which ensues is the following: when considering dozens of grains what is the effect of spatially stationary, irregularly positioned grains? Is the fluid's nonlinear behavior enhanced or damped by a disordered placements of identical disks? In a previous study on ordered and disordered porous media Lasseux, D., Abbasian Arani, A.A., Ahmadi, A. (2011) the same question was addressed for the case of weak and strong inertial effects, for a Newtonian fluid. Here the question can be posed when nonlinearities are induced by the viscosity law, focussing on the variation of the Darcy's effective permeability coefficients.

To answer the questions above we start by examining the case of a Carreau fluid with $n = 0.5$ and $\lambda = 5$, for a medium of porosity $\theta = 0.9$, with a driving pressure gradient inclined by $\alpha = 45^o$. Three different doubly periodic RVE's (*representative volume elements)* are used: 1×1, 2×2, and 3×3, with respectively, one, four and nine regularly arranged circular inclusions within the domain. In all cases the same results are found, i.e. $\mathcal{K}^C_{xx} = \mathcal{K}^C_{yy} = 0.0594$ and $\mathcal{K}^C_{xy} = \mathcal{K}^C_{yx} = 0.0070$.

Another test concerns the case of a RVE of dimensions 10×10, with 100 identical circular inclusions, arranged in either an orderly or a disorderly fashion. Two different fluids, with the same value of $n = 0.5$, are considered: one with $\lambda = 5$ and a second with $\lambda = 50$, to assess the effect of spatial disorder on both the case of weak and strong nonlinearities. Also, two values of the porosity θ are considered, while α is kept fixed at the value of zero degrees. The results are summarized in Table 3, and compared to the Newtonian case (for which $\lambda = 0$).

The grid employed is less dense in the 10×10 cases than in the single unit cell computations for reasons of available computer memory; nonetheless, the results permit to draw a few interesting considerations for both weakly nonlinear (WNL, $\lambda = 5$) and strongly nonlinear (SNL, $\lambda = 50$) fluids. The first is that, even for a 10×10 RVE, the components of $\mathbf{K}^C$ coincide with those found by using a single unit cell, in the ordered configuration. The possible exception appears to be the SNL case of the porous medium with large interstital spaces ($\theta = 0.9$), which displays a large permeability. In this configuration, however, the difference with respect to the reference 1×1 case is less than 1% for both components of the effective permeability; we believe that it should be ascribed to the relative inaccuracy in capturing large velocity gradients in the interstices of the medium, and thus the effective viscosity of the direct state. The same 1% error bar can be expected in the corresponding disordered case ($\lambda = 50, \theta = 0.9$). Regardless, it is clear that when the 100 grains are positioned randomly in the RVE (cf. Fig. 14) channeling of fluid through less resistive flow paths occurs, resulting in larger values of the permeability when the porosity is large. Such an excess is typically of order 10% for both WNL and SNL fluids. Conversely, when the porosity is $\theta = 0.6$, differences with respect to the reference, single-cell case are modest.

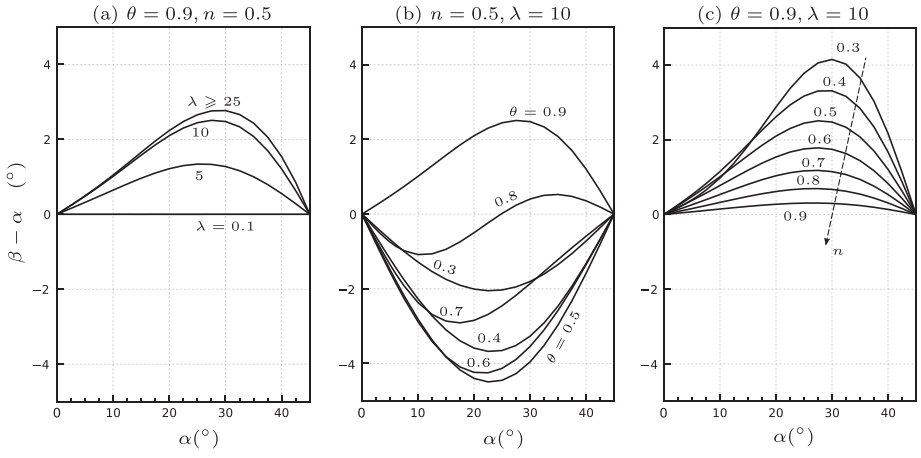

Fig. 13. Deviation angle $\beta - \alpha$ in degrees.

Table 3
Effective permeability components ($\mathcal{K}^C_{xx}$, $\mathcal{K}^C_{yy}$) for a single unit cell, and for the case of one hundred, ordered or disordered, cells. The off-diagonal components either vanish or are very small for a motion with $\alpha = 0^o$. The last two lines of the table provide the grid resolution for the two values of θ and for each configuration studied. The numbers in parentheses are (n_s, n_c), respectively the number of points along each side of the RVE, and the number of points on the boundary of each circular grain. The numbers in italics after the round brackets are the numbers of triangles used in each case.

λ	θ	Reference (1 × 1)	Ordered (10 × 10)	Disordered (10 × 10)
	0.9	(0.0403, 0.0403)	(0.0405, 0.0405)	(0.0433, 0.0449)
0	0.6	(0.0046, 0.0046)	(0.0046, 0.0046)	(0.0046, 0.0045)
	0.9	(0.0632, 0.0543)	(0.0636, 0.0546)	(0.0720, 0.0624)
5	0.6	(0.0055, 0.0046)	(0.0055, 0.0047)	(0.0055, 0.0048)
	0.9	(0.5437, 0.4266)	(0.5469, 0.4304)	(0.6318, 0.4886)
50	0.6	(0.0313, 0.0072)	(0.0314, 0.0072)	(0.0303, 0.0166)
	0.9	(240, 120), *66 544*	(120, 30), *131 554*	(240, 30), *141 762*
	0.6	(240, 120), *54 662*	(240, 60), *94 954*	(240, 60), *94 892*

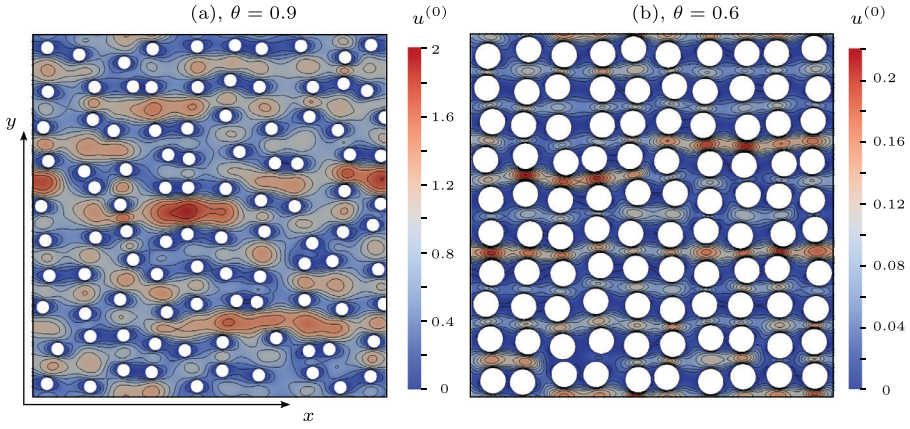

Fig. 14. Isolines of $u^{(0)}$ in a random 10 × 10 porous medium with $\theta = 0.9$ (a) and 0.6 (b), for a Carreau fluid with $\lambda = 50$ and $n = 0.5$. The pressure gradient is aligned with the horizontal axis in both cases.

6. Conclusions

Multi-scale homogenization has been used to study the creeping flow of a shear-thinning fluid, modelled through the Carreau viscosity law, in a porous medium. The leading order approximation of the direct, microscopic flow problem is non-linear because of the fluid rheology. By employing an "adjoint" approach, initiated by Bottaro Bottaro, A. (2019), we can easily address such a nonlinearity to find that, also for the case of non-Newtonian fluids, the macroscopic flow is ruled by Darcy's equation, as postulated by Zami-Pierre et al. Zami-Pierre, F., de Loubens, R., Quintard, M., Davit, Y. (2018). The important parameter in Darcy's equation is the effective permeability tensor, also denoted Carreau mobility or permeability. This is available by phase averaging the fields of an auxiliary (adjoint) problem in the unit cell. Because of the dependence of viscosity on the behavior of the fluid a strongly coupled solution must be pursued, and this coupling has a direct consequence on the anisotropy of the Carreau permeability, even for simple isotropic porous microstructures.

To highlight such an effect, consideration has been limited to the case of an elementary, two-dimensional porous geometry. Probably the main result of the work is that, except in limiting cases where the viscosity is close to Newtonian, the permeability cannot be reduced to a scalar quantity (despite the isotropicity of the geometrical configuration examined), so that the introduction of an effective (scalar) viscosity and the use of Eq. (1) leads to errors.

An extensive parametric analysis has been carried out to assess how the components of $\mathbf{K}^C$ vary with the rheological parameters λ and n, with the porosity of the material, θ, and with the direction of the macroscopic pressure gradient forcing the flow, expressed via the angle α. Low values of the power-law index n and large values of the time constant λ have the effect of significantly increasing the streamwise and transverse permeability components, as compared to their intrinsic counterpart. The off-diagonal component is also biased in an analogous manner and can grow to comparable magnitude, rendering the system strongly anisotropic. Anisotropicity can be assessed on the basis of a single scalar parameter, the anisotropy factor δ; whereas the variation of this factor is monotonic with respect to the two rheological constants, the behavior is non-trivial when analyzed with respect to the geometry of the porous medium (expressed via θ) and the inclination angle of the pressure gradient, α. This appears to represent an obstacle to the development of simplified models of the flow of shear-thinning fluids in porous media. However, the deviation of the mean flow with respect to the macroscopic pressure gradient is consistently limited to a few degrees for a wide range of parameters, so that approximating it to zero should constitute an acceptable approximation.

Finally, when a large *representative volume element* is considered, with grains positioned randomly within the available space, differences of the order of about 10% in the values of the apparent permeability components occur primarily when the porosity is very large, when comparing to the corresponding single-cell values. For intermediate and low porosity values the disordered arrangement of the solid inclusions seems to yield a negligible effect. This issue deserves to be investigated further, particularly for three-dimensional configurations.

Declaration of competing interest

The authors declare that they have no conflicts of interest.

Acknowledgements

This work has benefited from an "*Attractivity Chair*" granted by the University of Toulouse to AB in the frame of a program by the IDEX Foundation. Useful discussions with Michel Quintard and Yohan Davit are gratefully acknowledged.

Table A1
Convergence analysis for a Newtonian fluid in a medium of porosity $\theta = 0.9$. Left: first component of the tensor $\mathcal{K}^C$ for the three different grids tested. Right: grid convergence metrics ($\hat{p} \approx 3.215$).

mesh index	mesh identifier	$100 \times \mathcal{K}^C_{xx}$		metric	value
3	fine	4.02728	GCI_{23}	0.040%	
2	medium	4.02777	GCI_{12}	0.060%	
1	coarse	4.02857	$AC - 1$	2.4×10^{-4}	

Appendix A. Numerical convergence

The grid convergence analysis has been performed with the *GCI* approach introduced by Roache (1998), also employed in our previous recent study Luminari, N., Airiau, C., Bottaro, A. (2018). The method is based upon a grid refinement error estimator derived from the theory of generalized Richardson extrapolation. It measures the ratio between the computed value of a quantity over the asymptotic numerical value, thus indicating how far the solution is from the asymptotic ("exact") value. The procedure is simple and provides a method to estimate the order of the spatial convergence, based on two or three different grid sizes. Four steps must be followed, outlined below.

1. Estimate the order of convergence of the procedure, defined as $\hat{p} = \dfrac{\ln \dfrac{f_3 - f_2}{f_2 - f_1}}{\ln r}$, where r is the grid refinement ratio between each grid (it is computed as the ratio between the number of elements of two consecutive grids; the approach imposes that r should remain quasi-constant between any couple of consecutive grids and be larger than 1.1). For the present study the quantity f_i is given by the $\mathcal{K}^C_{xx}$ component; the subscripts are: $i = 1$ for the coarse grid, $i = 2$ for the medium grid, and $i = 3$ for the fine grid. The number of elements of each one of these grids is given in section 4.
2. Compute the relative error between grid i and j: $|\epsilon|_{ij} = \dfrac{f_j - f_i}{f_i}$, for $(i, j) \in \{(1, 2), (2, 3)\}$.
3. Compute $GCI_{ij} = \dfrac{F_s |\epsilon|_{ij}}{r^{\hat{p}} - 1}$, with F_s a factor which can be taken equal to 1.25 when three grids are used, according to Roache's prescription Roache (1998).
4. Check whether each grid level yields a solution that is in the asymptotic range of convergence; this means that the coefficient $AC = \dfrac{GCI_{23}}{GCI_{12}} \dfrac{1}{r^{\hat{p}}}$ should be as close as possible to one.

The results for the case of a Newtonian fluid are reported in Table A1. It is clear that the coarser mesh, employed throughout this paper for the unit cell case, is more than adequate for our purposes. The same convergence analysis conducted for the case of Carreau fluids, varying the model parameters, yields the same conclusion on the adequacy of the grid employed.

Supplementary material

Supplementary material associated with this article can be found, in the online version, at doi:10.1016/j.advwatres.2020.103658.

References

BalhoffM.T., Thompson, K.E., 2006. A macroscopic model for shear-thinning flow in packed beds based on network modeling. Chem. Eng. Sci. 61 (2), 698–719. https://doi.org/10.1016/j.ces.2005.04.030.

BedfordA., Drumheller, D.S., 1983. Theories of immiscible and structured mixtures. Int. J. Engng Sci. 21, 863–960. https://doi.org/10.1023/A:1006647505709.

BergS., van Wunnink, J., 2017. Shear rate determination from pore-scale flow fields. Trans. Por. Media 117 (2), 229–246. https://doi.org/10.1007/s11242-017-0830-3.

BirdR.B., Armstrong, R.C., Hassager, O., 1987. *Dynamics of polymeric liquids. vol. 1, fluid mechanics*, 2nd ed.. Wiley-Interscience, NY.

BottaroA., 2019. Flow over natural or engineered surfaces: an adjoint homogenization perspective. J. Fluid Mech. 877, p.1–91. https://doi.org/10.1017/jfm.2019.607.

BourgeatA., Mikelić, A., 1993. Note on the homogenization of bingham flow through porous media. J. Math. Pures Appl. 72, 405–414.

BourgeatA., Mikelić, A., 1996. Homogenization of a polymer flow through a porous medium. Nonlinear Anal. Theory, Meth. Appl. 26 (7), 1221–1253. https://doi.org/10.1016/0362-546X(94)00285-P.

BrezziF., Falk, R., 1991. Stability of higher order taylor-hodd methods. SIAM J. Numer. Anal. 28 (3), 581–590. https://doi.org/10.1137/0728032.

Cannella, W.J., Huh, C., Seright, R.S.,. Prediction of xanthan rheology in porous media. SPE 18089. Paper presented at the 63rd Annual Technical Conference and Exhibition of the Society of Petroleum Engineers, Houston, TX, Oct. 2–5, 1988. . 10.2118/18089-MS.

Carreau, P.J., 1972. Rheological equations from molecular network theories. Trans. Soc. Rheol. 16 (1), 99–127. https://doi.org/10.1122/1.549276.

ChenL., 2014. A simple construction of a fortin operator for the two dimensional taylorhood element. Computer & Mathematics with Applications 68 (10), 1368–1373. https://doi.org/10.1016/j.camwa.2014.09.003.

ChristopherR.H., Middleman, S., 1965. Power-law flow through a packed tube. Ind. Eng. Chem. Res. 4, 422–426. https://doi.org/10.1021/i160016a011.

CowinS.C., Cardoso, L., 2015. Blood and interstitial flow in the hierarchical pore space architecture of bone tissue. J. Biomech. 48 (5), 842–854. https://doi.org/10.1016/j.jbiomech.2014.12.013.

DavitY., Bell, C.G, Byrne, H.M., Chapman, L.A.C., Kimpton, L.S., Lang, G.E., Leonard, K.H.L., Oliver, J.M., Pearson, N.C., Shipley, R.J., Waters, S.L., Whiteley, J.P., Wood, B.D., Quintard, M., 2013. Homogenization via formal multiscale asymptotics and volume averaging: how do the two techniques compare? Adv. Water Res. 62–Part B, 178–206. https://doi.org/10.1016/j.advwatres.2013.09.006.

EberhardU., Seybold, H.J., Floriancic, M., Bertsch, P., Jiménez-Martínez, J., Andrade J.S. Jr., Holzner, M., 2019. Determination of the effective viscosity of non-newtonian fluids flowing through porous media. Front. Phys. 7, 71(1–9). https://doi.org/10.3389/fphy.2019.00071.

GötzT., Parhusip, H.A., 2005. On an asymptotic expansion for carreau fluids in porous media. J. Eng. Math. 51 (4), 351–365. https://doi.org/10.1007/s10665-004-7468-1.

GreenD.W., Willhite, G.P., 2018. *Enhanced oil recovery*, 2nd ed.. Society of Petroleum Engineers, Richardson, TX, USA.

HechtF., 2012. New development in freefem++. J. Num. Math. 20 (3–4), 251–266. https://doi.org/10.1515/jnum-2012-0013.

HirasakiG.J., Pope, G.A., 1974. Analysis of factors influencing mobility and adsorption in the flow of polymer solution through porous media. Soc. Petrol. Eng. 14, 337–346. https://doi.org/10.2118/4026-PA.

HouM.Z., Xie, H., Were, P., Eds., 2013. *Clean energy systems in the subsurface: production, storage and conversion*. proceedings of the 3rd sino-German conference 'underground storage of CO2 and Energy', goslar, germany, 21–23 may 2013. Springer-Verlag, Berlin, Germany https://doi.org/10.1007/978-3-642-37849-2.

IdrisZ., Orgéas, L., Geindreau, C., Bloch, J.-F., Auriault, J.-L., 2004. Microstructural effects on the flow law of power-law fluids through fibrous media. Modelling Simul. Mater. Sci. Eng. 12 (5), 995–1015. https://doi.org/10.1088/0965-0393/12/5/016.

KozenyJ., 1927. Über kapillare leitung des wassers im boden. Sitzungsber. Akad. Wiss., Wien 136, 271–306.

LasseuxD., Abbasian Arani, A.A., Ahmadi, A., 2011. On the stationary macroscopic inertial effects for one phase flow in ordered and disordered porous media. Phys. Fluids 23, 073103. https://doi.org/10.1063/1.3615514.

LionsJ.L., Sanchez-Palencia, E., 1981. Écoulement d'un fluid viscoplastique de bingham dans un milieu poreux. J. Math. Pures Appl. 60, 341–360.

Lodge A.S., 1968. Constitutive equations from molecular network theories for polymer solutions. Rheol. Acta 7 (4), 379–392. https://doi.org/10.1007/BF01984856.

LuminariN., Airiau, C., Bottaro, A., 2018. Effects of porosity and inertia on the apparent permeability tensor in fibrous media. Int. J. Multiph. Flow 106, 60–74. https://doi.org/10.1016/j.ijmultiphaseflow.2018.04.013.

MarxN., Fernández, L., Barceló, F., Spikes, H., 2018. Shear thinning and hydrodynamic friction of viscosity modifier-containing oils. Part I: Shear thinning behaviour. Trib. Lett. 66, 92(1–14). 0.1007/s11249-018-1039-5

McCain Jr.W.D., 1990. *The properties of petroleum fluids*, 2nd ed.. PennWell Books, Tulsa, OK, USA.

McKinleyR.M., Jahns, H.O., Harris, W.W., Greenkorn, R.A., 1966. Non-newtonian flow in porous media. AIChE J. 12 (1), 17–20. https://doi.org/10.1002/aic.690120106.

MeiC.C., Vernescu, B., 2010. *Homogenization methods for multiscale mechanics*. World Scientific Publishing Co., Singapore. https://doi.org/10.1142/7427.

MikelićA., 2000. Homogenization theory and applications to filtration through porous media. In: A. Fasano (ed.), Filtration in Porous Media and Industrial Applications, Lectures given at the 4th Session of the Centro Internazionale Matematico Estivo (C.I.M.E.) held in Cetraro, Italy, August 24–29, 1998. Issue 1734, 93–214. https://doi.org/10.1007/BFb0103977.

OrgéasL., Geindreau, C., Auriault, J.-L., Bloch, J.-F., 2007. Upscaling the flow of generalized newtonian fluids through anisotropic porous media. J. Non-Newtonian Fluid Mech. 145, 15–29. https://doi.org/10.1016/j.jnnfm.2007.04.018.

OrgéasL., Idris, Z., Geindreau, C., Bloch, J.-F., Auriault, J.-L., 2006. Modelling the flow of power-law fluids through anisotropic porous media at low-pore reynolds number. Chem. Eng. Sci. 61 (14), 4490–4502. https://doi.org/10.1016/j.ces.2006.01.046.

OstwaldW., 1925. Über die geschwindigkeitsfunktion der viskosität disperser systeme. i. Kolloid-Zeitschrift 36 (2), 99–117. https://doi.org/10.1007/BF01431449.

OstwaldW., 1929. Über die rechnerische darstellung des strukturgebietes der viskosität. Kolloid-Zeitschrift 47 (2), 176–187. https://doi.org/10.1007/BF01496959.

QuintardM., Whitaker, S., 1993. Transport in ordered and disordered porous media: volume-averaged equations, closure problems, and

comparison with experiment. Chem. Eng. Sci. 48 (14), 2537–2564. https://doi.org/10.1016/0009-2509(93)80266-S.

QuintardM., Whitaker, S., 1994. Transport in ordered and disordered porous media i: the cellular average and the use of weighting functions. Trans. Por. Media 14 (2), 163–177. https://doi.org/10.1007/BF00615199.

QuintardM., Whitaker, S., 1994. Transport in ordered and disordered porous media II: generalized volume averaging. Trans. Por. Media 14 (2), 179–206. https://doi.org/10.1007/BF00615200.

Roache, P.J., 1998. Verification and validation in computational science and engineering. Hermosa Press, Albuquerque, NM..

Rodriguez de CastroA., Radilla, G., 2017. Non-darcian flow of shear-thinning fluids through packed beads: experiments and predictions using forchheimer's law and ergun's equation. Adv. Water Res. 100, 35–47. https://doi.org/10.1016/j.advwatres.2016.12.009.

SadowskiT.J., Bird, R.G., 1965. Non-newtonian flow through porous media. i. theoretical. Trans. Soc. Rheol. 9, 243–250. https://doi.org/10.1122/1.549000.

ShahsavariS., McKinley, G.H., 2015. Mobility of power-law and carreau fluids through fibrous media. Phys. Rev. E 92 (6), 63012. https://doi.org/10.1103/PhysRevE.92.063012.

TannerR.I., 2000. *Engineering rheology*, 2nd ed.. Oxford University Press, Oxford, UK.

WangX.-H., Jia, J.-T., Liu, Z.-F., Jin, L.-D., 2014. Derivation of the darcy-scale filtration equation for power-law fluids with the volume averaging method. J. Por. Media 17 (8), 741–750. https://doi.org/10.1615/JPorMedia.v17.i8.80.

WhitakerS., 1986. Flow in porous media i: a theoretical derivation of darcy's law. Trans. Por. Media 1 (1), 3–25. https://doi.org/10.1007/BF01036523.

Zami-PierreF., de Loubens, R., Quintard, M., Davit, Y., 2016. Transition in the flow of power-law fluids through isotropic porous media. Phys. Rev. Letters 117 (7), 074502. https://doi.org/10.1103/PhysRevLett.117.074502.

Zami-PierreF., de Loubens, R., Quintard, M., Davit, Y., 2018. Effect of disorder in the pore-scale structure on the flow of shear-thinning fluids through porous media. J. Non-Newtonian Fluid Mech. 261, 99–110. https://doi.org/10.1016/j.jnnfm.2018.08.004.

ZampognaG., Bottaro, A., 2016. Fluid flow over and through a regular bundle of rigid fibres. J. Fluid Mech. 792, p.5–35. https://doi.org/10.1017/jfm.2016.66.